GEOPHYSICS, VOL. 86, NO. 4 (JULY-AUGUST 2021); P. T179–T192, 16 FIGS.
10.1190/GEO2020-0659.1

Eulerian partial-differential-equation methods for complex-valued eikonals in attenuating media

Jiangtao Hu[1], Jianliang Qian[2], Jian Song[2], Min Ouyang[3], Junxing Cao[1], and Shingyu Leung[4]

ABSTRACT

Seismic waves in earth media usually undergo attenuation, causing energy losses and phase distortions. In the regime of high-frequency asymptotics, a complex-valued eikonal is an essential ingredient for describing wave propagation in attenuating media, where the real and imaginary parts of the eikonal function capture dispersion effects and amplitude attenuation of seismic waves, respectively. Conventionally, such a complex-valued eikonal is mainly computed either by tracing rays exactly in complex space or by tracing rays approximately in real space so that the resulting eikonal is distributed irregularly in real space. However, seismic data processing methods, such as prestack depth migration and tomography, usually require uniformly distributed complex-valued eikonals. Therefore, we have developed a unified framework to Eulerianize several popular approximate real-space ray-tracing methods for complex-valued eikonals so that the real and imaginary parts of the eikonal function satisfy the classic real-space eikonal equation and a novel real-space advection equation, respectively, and we dub the resulting method the Eulerian partial-differential-equation method. We further develop highly efficient high-order methods to solve these two equations by using the factorization idea and the Lax-Friedrichs weighted essentially nonoscillatory schemes. Numerical examples demonstrate that our method yields highly accurate complex-valued eikonals, analogous to those from ray-tracing methods. Our methods can be useful for migration and tomography in attenuating media.

INTRODUCTION

Because of the influence of material properties and fractures and because of the porosity and granularity of subsurface rocks, seismic wave propagation in earth media is intrinsically attenuating (Aki and Richards, 1980; Červený, 2001; Carcione, 2015). Without properly accounting for attenuation effects, seismic data processing may produce unreliable delineation of geologic structures. Therefore, it is crucial to develop efficient modeling methods for wave propagation in attenuating media. On one hand, although direct modeling methods such as finite-difference and finite-element methods are highly accurate, they are sometimes computationally expensive to use (Robertsson et al., 1994; Blanch et al., 1995; Blanch and Robertsson, 1997; Carcione, 1999, 2009; Carcione et al., 2002; Zhang et al., 2010; Xie et al., 2015); on the other hand, although ray methods (Gajewski and Pšenčik, 1992; Červený, 2001; Vavryčuk, 2008a; Hao and Alkhalifah, 2017; Huang and Greenhalgh, 2018; Huang et al., 2018) are of lower accuracy in comparison to direct methods, they are highly efficient and are able to provide adequate accuracy for many geophysical scenarios. Consequently, we seek high-frequency asymptotic ray-theory methods to develop efficient numerical tools for modeling attenuating wave motions. Consider applying such an asymptotic method to viscoelastic isotropic wave equations with complex-valued frequency-dependent elastic parameters. Vanishing the leading-order singularity in terms of the reciprocal of large frequency yields the complex eikonal equations satisfied by the complex-valued eikonal functions for the P- and S-wave, respectively. Then, the question reduces to how to solve such a complex eikonal equation efficiently. In this

Manuscript received by the Editor 4 September 2020; revised manuscript received 26 January 2021; published ahead of production 25 March 2021; published online 1 June 2021.
[1]State Key Laboratory of Oil and Gas Reservoir Geology and Exploitation (Chengdu University of Technology), No. 1, Dongsanlu, Erxianqiao, Chengdu 610059, China. E-mail: jiangtao_hu@126.com (corresponding auhtor); caojx@cdut.edu.cn.
[2]Michigan State University, Department of Mathematics and Department of CMSE, East Lansing, Michigan 48824, USA. E-mail: jqian@msu.edu; songji12@msu.edu.
[3]Zhanjiang Branch of CNOOC Limited, Zhanjiang 524000, China. E-mail: ouyangm@cnooc.com.cn.
[4]Hong Kong University of Science and Technology, Department of Mathematics, Hong Kong SAR 999077, China. E-mail: masyleung@ust.hk.

paper, we propose a unified framework to Eulerianize several popular real-space Lagrangian ray-tracing methods so that we can develop efficient Eulerian partial-differential-equation (PDE) methods for computing complex-valued eikonals, in which the real and imaginary parts of the eikonal function describe wave propagation and attenuation effects, respectively.

As a first-order nonlinear PDE, the complex eikonal equation can be solved by the method of characteristics to yield complex-valued eikonal functions, leading to the so-called complex-space ray-tracing method, which theoretically enables us to solve the complex eikonal equation without any approximation. However, because sources and receivers are usually located in real space in most applications, the complex-space ray-tracing method brings about unusual complications in that rays are now situated in complex space so that the dimension of the ambient space becomes doubled; consequently, the resulting ray-tracing system is high-dimensional and is costly to solve. Moreover, it is hard to build complex-valued elastic-parameter models from real-valued models that are usually available from measurements in real space (Vavryčuk, 2008a; Hao and Alkhalifah, 2017). Therefore, some further approximations are pursued to develop real-space ray-tracing methods for computing complex-valued eikonal functions.

In viscoacoustic media, the widely used weakly attenuating approximation (i.e., the inverse of quality factor $\ll 1$) (Gajewski and Pšenčik, 1992; Červený, 2001; Keers et al., 2001; Xie et al., 2009; Xin et al., 2014; Hu et al., 2018) can be used to reduce the complex-space ray-tracing system to a real-space ray-tracing system approximately in terms of the quality factor. Numerical experiments in Gajewski and Pšenčik (1992) demonstrate that the weakly attenuating assumption is applicable to a substantial range of quality factors encountered in exploration geophysics. Keers et al. (2001) show that the raypath under the weakly attenuating approximation is identical to that in the corresponding nonattenuating medium, so that the ray-tracing method in a nonattenuating medium can be used to obtain the real and imaginary parts of the complex-valued eikonal, where the ray-tracing system is defined in real space because the reference velocity and quality factor are real. In this approximate real-space ray-tracing model, the real and imaginary parts of the complex-valued eikonal at each receiver have to be found indirectly via solving nonlinear systems or numerical quadratures.

Viewing a viscoelastic medium as the perturbation of a perfectly elastic medium, one may account for attenuation effects by using the first-order perturbations and tracing rays in the elastic reference medium that is specified in real space (Vavryčuk, 2008b; Klimeš and Klimeš, 2011; Hao and Alkhalifah, 2017). Vavryčuk (2012) calls this method the real-elastic ray-tracing method. Here again the real part of the complex-valued eikonal at each receiver has to be found indirectly, and, accordingly, the corresponding imaginary part has to be found from numerical quadratures.

Another real-space ray-tracing method for viscoelastic media, the real viscoelastic ray-tracing method, is proposed by Vavryčuk (2008a). This method modifies the Hamiltonian for viscoelastic media so that the rays are constrained as trajectories in real space (Vavryčuk, 2012). The resulting ray-tracing system is based on a certain real-valued reference velocity calculated from the complex-valued phase velocity for the P- or S-wave, respectively. Although this approach is still approximate, this method is highly accurate and is applicable to strongly attenuating media (Vavryčuk, 2012; Hao and Alkhalifah, 2017), where the real and imaginary parts of the complex-valued eikonal are obtained in the same way as the real elastic ray-tracing method.

To date, because all of the rays are traced from an arbitrary source point to receivers by solving an initial value problem for ordinary differential equations (ODEs), all of these real-space ray-tracing methods yield the real and imaginary parts of the complex-valued eikonal at irregularly distributed points, and such irregular distributions of complex-valued eikonals hinder their applications to seismic migration and tomography because these applications are usually posed on regular mesh points. Therefore, we are motivated to develop efficient methods to produce complex-valued eikonals on regular grids by formulating the above three real-space ray-tracing systems into PDEs.

Assuming that there is a unique ray connecting any source to any receiver, one possibility is to solve an eikonal equation with an appropriate reference velocity for the real part of the complex-valued eikonal and solve an advection equation with an appropriate quality-factor function for the imaginary part of the complex-valued eikonal, where the advection equation is weakly coupled to the eikonal equation in the sense that the advection coefficients are defined by the gradient of the real part of the complex-valued eikonal; the resulting Eulerian method yields a single-valued approximate solution for the complex eikonal equation. Because the unique-ray assumption is very restrictive, we in fact will solve the aforementioned eikonal equation for the real part in the sense of a viscosity solution (Lions, 1982; van Trier and Symes, 1991) so that our resulting computation is with the first-arrival-based real part of the complex-valued eikonal.

Now the question is how to solve the weakly coupled eikonal and advection equations efficiently with high-order accuracy so as to obtain the real and imaginary parts of the complex-valued eikonal. Supposing that we wish to compute the imaginary part to first-order accuracy, which is in fact a minimum requirement, we need to have at least a first-order accurate gradient of the real part because the numerically differentiated gradient of the real part serves as coefficients for the advection equation satisfied by the imaginary part. This in turn implies that the computed real part be of at least second-order accuracy so that its numerical gradient is of first-order accuracy; the consequence is that we need high-order accurate eikonal solvers. Such an accuracy requirement has been first observed by Qian and Symes (2002a) for solving transport equations of amplitudes. Although first-order accurate eikonal solvers are abundant (Vidale, 1988; Podvin and Lecomte, 1991; van Trier and Symes, 1991; Qin et al., 1992; Pica, 1997; Sethian and Popovici, 1999; Qian and Symes, 2002a; Kao et al., 2004, 2008; Zhang et al., 2005; Zhao, 2005; Qian et al., 2007a, 2007b; Fomel et al., 2009; Serna and Qian, 2010; Luo and Qian, 2012; Waheed et al., 2015), only a few high-order accurate point-source eikonal solvers are available (Kim and Cook, 1999; Qian and Symes, 2002a; Zhang et al., 2006; Serna and Qian, 2010; Luo et al., 2014; Lu et al., 2016; Qian et al., 2016). Following the work in Qian et al. (2016) in which the eikonal and transport equations are solved to high-order accuracy with proper initializations at the point source, we develop high-order Lax-Friedrichs weighted essentially nonoscillatory (LxF-WENO) schemes for the eikonal and advection equations under consideration. The WENO approximation of derivatives (Jiang and Peng, 2000; Qian et al., 2016) provides better numerical stability when complex wavefronts are encountered. Moreover, the point-source singularities of the eikonal and advection equations are

treated by systematic factorizations (Pica, 1997; Zhang et al., 2005; Fomel et al., 2009; Luo et al., 2014; Lu et al., 2016; Qian et al., 2016).

The rest of the paper is organized as follows. In the "Methodology" section, we propose a unified framework to compute the real and imaginary parts of the complex-valued eikonal, and we put three popular real-space ray-tracing models for viscous wave motion into this framework; we further develop factorized PDEs to solve the resulting eikonal and advection equations by using the LxF-WENO schemes. Numerical experiments demonstrate the feasibility of the proposed method.

METHODOLOGY

Eulerian PDE framework for complex-valued traveltimes

The correspondence principle indicates that we can treat wave propagation in a viscoelastic (or viscoacoustic) medium as wave propagation through an elastic (or acoustic) medium with complex-valued elastic parameters (or a complex-valued velocity). To model wave motion in such a medium efficiently, high-frequency asymptotic approximations provide an effective alternative to direct numerical methods. One of the essential ingredients for high-frequency asymptotics of viscous wave motion is the complex-valued eikonal function. We propose a unified Eulerian framework to compute complex-valued eikonal functions for several popular high-frequency asymptotic models of viscous wave motions.

We assume that the complex-valued eikonal function τ consists of the real part T and the imaginary part T^*, which satisfy the following eikonal and advection equation, respectively:

$$|\nabla T| = \frac{1}{v(\mathbf{x})}, \quad T(\mathbf{x}_s) = 0, \tag{1}$$

$$\nabla T \cdot \nabla T^* = \frac{1}{v^2(\mathbf{x})Q(\mathbf{x})}, \quad T^*(\mathbf{x}_s) = 0, \tag{2}$$

where $\mathbf{x}$ is the real-valued position vector, $v(\mathbf{x})$ is the real-valued reference velocity, and $Q(\mathbf{x})$ is a quality-factor-related real-valued function.

Assuming that there is a unique ray connecting any source to any receiver, we put three popular asymptotic models into our framework. Provided that we choose an appropriate reference velocity and an appropriate quality-factor related function, our framework is applicable to weakly and strongly attenuating media.

Case 1: Viscoacoustic ray tracing and Eulerian equations

Wave motion in a viscoacoustic medium can be characterized as wave propagation through an acoustic medium with a complex-valued velocity. The complex-valued velocity is given in terms of the real acoustic velocity c_0 and the quality factor q, the latter representing the attenuation. If the attenuation is small ($q^{-1} \ll 1$, the weakly attenuating approximation), then an appropriate definition of the complex-valued velocity c is

$$c(\mathbf{x}) = c_0(\mathbf{x})\left[1 + \frac{1}{2}\frac{i}{q(\mathbf{x})} + \frac{1}{\pi}\ln\left(\frac{\omega}{\omega_0}\right)\right], \tag{3}$$

where ω is the angular frequency, ω_0 is a reference angular frequency, and the dispersive term in the real part of the velocity ensures causality of wave-equation solutions (Aki and Richards, 1980).

If $q^{-1} \ll 1$, then to the first-order approximation in q^{-1}, the raypaths defined in the high-frequency approximation by the real acoustic velocity c_0 can be considered to be unaffected by attenuation and remain unchanged during the viscoacoustic wave motion, but the traveltime function becomes complex valued and frequency dependent due to the attenuation effect, which takes the following form by Futterman's dispersion relation (Futterman, 1962; Gajewski and Pšenčík, 1992; Červený, 2001; Keers et al., 2001):

$$T_c(\mathbf{x}) = T(\mathbf{x}) - \frac{1}{\pi}T^*(\mathbf{x})\ln\left(\frac{\omega}{\omega_0}\right) - i\frac{T^*(\mathbf{x})}{2}, \tag{4}$$

where

$$T(\mathbf{x}) = \int_{\text{ray}} \frac{1}{c_0(\mathbf{x})}\,ds, \tag{5}$$

$$T^*(\mathbf{x}) = \int_{\text{ray}} \frac{1}{c_0(\mathbf{x})q(\mathbf{x})}\,ds. \tag{6}$$

Here, T is the traveltime in acoustic media from the source $\mathbf{x}_s$ to $\mathbf{x}$, and it satisfies the following eikonal equation:

$$|\nabla T(\mathbf{x})| = \frac{1}{c_0(\mathbf{x})}; \tag{7}$$

the arc-length integrations in equations 5 and 6 are over the same raypath connecting the source $\mathbf{x}_s$ to $\mathbf{x}$ defined by the real acoustic velocity c_0. The raypath can be either determined by Fermat's principle or implicitly defined by solving the eikonal equation 7. Because the directional derivative along the raypath defined in equation 7 is (Lu et al., 2016)

$$\frac{\partial}{\partial s} = c_0(\mathbf{x})\nabla T(\mathbf{x}) \cdot \nabla, \tag{8}$$

we can take the directional derivative along the raypath on both sides of equation 6 to have the following advection equation for T^*:

$$\nabla T(\mathbf{x}) \cdot \nabla T^*(\mathbf{x}) = \frac{1}{c_0^2(\mathbf{x})q(\mathbf{x})}. \tag{9}$$

This corresponds to our case that $v(\mathbf{x}) = c_0(\mathbf{x})$ and $Q(\mathbf{x}) = q(\mathbf{x})$ in equations 1 and 2.

Case 2: Real viscoelastic ray tracing and Eulerian equations

Wave motion in a viscoelastic medium can be described by a real-valued density ρ of the medium, complex-valued and frequency-dependent Lamé elastic coefficients λ and μ, and a real-valued angular frequency. The real parts, λ^R and μ^R, describe the elastic properties of the medium, and the imaginary parts, λ^I and μ^I, describe the attenuation. The P- and S-wave velocities, respectively,

DOI:10.1190/geo2020-0659.1

$$c_{\mathrm{P}} = \sqrt{\frac{\lambda + 2\mu}{\rho}}, \quad c_{\mathrm{S}} = \sqrt{\frac{\mu}{\rho}}, \tag{10}$$

are complex-valued and frequency-dependent. The strength of attenuation is evaluated using the quality factor for the P- and S-wave (Carcione, 2015), respectively,

$$q_{\mathrm{P}} = -\frac{\lambda^R + 2\mu^R}{\lambda^I + 2\mu^I} = -\frac{(c_{\mathrm{P}}^2)^R}{(c_{\mathrm{P}}^2)^I}, \quad q_{\mathrm{S}} = -\frac{\mu^R}{\mu^I} = -\frac{(c_{\mathrm{S}}^2)^R}{(c_{\mathrm{S}}^2)^I}. \tag{11}$$

Vavryčuk (2008b, 2012) proposes to solve the P- and S-wave complex-valued eikonal equations using real ray-tracing methods, and such methods modify the Hamiltonians for viscoelastic media so as to keep rays as trajectories in real space. The resulting real viscoelastic ray-tracing equations in isotropic media are (Vavryčuk, 2008b)

$$\frac{d\mathbf{x}}{d\tau^R} = V^2\mathbf{p}, \quad \frac{d\mathbf{p}}{d\tau^R} = -\frac{1}{V}\nabla V, \quad \frac{d\tau^I}{d\tau^R} = -\frac{c^I}{c^R}, \tag{12}$$

where $\mathbf{p}$ is the slowness vector, τ^R and τ^I are the real and imaginary parts of the complex eikonal, respectively, c^R and c^I are the real and imaginary parts of the complex velocity, respectively, and V is the real-valued ray velocity calculated from the complex-valued phase velocity,

$$V = \frac{1}{(c^{-1})^R} = \frac{(c^R)^2 + (c^I)^2}{c^R}, \tag{13}$$

with $c = c_{\mathrm{P}}$ or $c = c_{\mathrm{S}}$ for the P- or S-wave, respectively.

The real part of the complex-valued eikonal, τ^R, of the ray-tracing system in equation 12 satisfies the following eikonal equation:

$$|\nabla\tau^R| = \frac{1}{V(\mathbf{x})}. \tag{14}$$

The imaginary part of the complex-valued eikonal τ^I takes the following integration form:

$$\tau^I(\mathbf{x}) = \int_{\mathrm{ray}} -\frac{c^I(\mathbf{x})}{V(\mathbf{x})c^R(\mathbf{x})}ds. \tag{15}$$

Similar to the viscoacoustic ray-tracing case, using the directional derivative defined by equation 14 to take the directional derivative along the raypath on both sides of equation 15, we can have the following advection equation for the imaginary part of the complex-valued eikonal, τ^I:

$$\nabla\tau^R \cdot \nabla\tau^I = -\frac{c^I(\mathbf{x})}{V^2(\mathbf{x})c^R(\mathbf{x})}. \tag{16}$$

This corresponds to our case that $T = \tau^R$, $T^* = \tau^I$, $v(\mathbf{x}) = V(\mathbf{x})$, and $Q(\mathbf{x}) = -((c^R(\mathbf{x}))/(c^I(\mathbf{x})))$ in equations 1 and 2.

Case 3: Real elastic ray tracing and Eulerian equations

In the real elastic ray-tracing theory, a viscoelastic medium is considered as the perturbation of a perfectly elastic medium so that the rays are traced in the elastic reference medium and the effects of attenuation are calculated by first-order perturbations. The resulting real elastic ray-tracing equations are (Červený, 2001)

$$\frac{d\mathbf{x}}{d\tau^R} = V_0^2\mathbf{p}, \quad \frac{d\mathbf{p}}{d\tau^R} = -\frac{1}{V_0}\nabla V_0, \quad \frac{d\tau^I}{d\tau^R} = \frac{1}{2q}, \tag{17}$$

where V_0 is the real-valued reference velocity in the reference elastic medium. Gajewski and Pšenčik (1992) take the weakly attenuating approximation and ignore $(c^I)^2$ in equation 13, and V_0 becomes

$$V_0 = c^R, \tag{18}$$

with $c^R = (c_{\mathrm{P}})^R$ and $q = q_{\mathrm{P}}$ or $c^R = (c_{\mathrm{S}})^R$ and $q = q_{\mathrm{S}}$ for the P- or S-wave, respectively.

Similar to the real viscoelastic ray-tracing case, we can have the following eikonal and advection equations for the real part, τ^R, and the imaginary part, τ^I, of the complex-valued eikonal, respectively,

$$|\nabla\tau^R| = \frac{1}{V_0(\mathbf{x})}, \tag{19}$$

$$\nabla\tau^R \cdot \nabla\tau^I = \frac{1}{2q(\mathbf{x})V_0^2(\mathbf{x})}. \tag{20}$$

This corresponds to our case that $T = \tau^R$, $T^* = \tau^I$, $v(\mathbf{x}) = V_0(\mathbf{x})$, and $Q(\mathbf{x}) = 2q(\mathbf{x})$ in equations 1 and 2.

Factorized Eulerian PDEs

Finite-difference schemes to the point-source eikonal equation 1 are widely used (Vidale, 1988; Podvin and Lecomte, 1991; van Trier and Symes, 1991; Qin et al., 1992; Qian and Symes, 2002a), but without proper treatment of the point-source singularity, most of these schemes only yield low accuracy near the source point (Qian and Symes, 2002a). Such initial errors at the source will spread out to the entire computational domain due to the upwind nature of these schemes (Qian and Symes, 2002a). Adaptive refinement near the source (Qian and Symes, 2002a) and factorizing out the point-source singularity explicitly from the point-source eikonal (Pica, 1997; Zhang et al., 2005; Fomel et al., 2009; Luo and Qian, 2012; Luo et al., 2014; Lu et al., 2016; Qian et al., 2016) provide two effective strategies for treating this singularity. Moreover, comparing equation 2 with equation 1, we realize that the imaginary part of the complex eikonal shares a similar singularity with the real part of the complex eikonal so that we will apply the factorization idea as well to the advection equation to treat the source singularity.

We adopt a multiplicative factorization (Pica, 1997; Zhang et al., 2005; Fomel et al., 2009; Luo and Qian, 2012; Lu et al., 2016; Qian et al., 2016) to the real part of the complex eikonal,

$$T(\mathbf{x}) = \tau_0(\mathbf{x})\tau_1(\mathbf{x}), \tag{21}$$

where τ_0 is the analytic traveltime function for a known homogeneous velocity model, which captures the source singularity, and the unknown factor τ_1 is computed from a finite-difference scheme. The analytic factor τ_0 is taken to be

$$\tau_0(\mathbf{x}) = \frac{|\mathbf{x} - \mathbf{x}_s|}{v_s}, \tag{22}$$

where v_s is the velocity at the source location, and this choice corresponds to the first-order factorization (Lu et al., 2016; Qian et al., 2016). Inserting equation 21 into equation 1, we obtain the factored eikonal equation:

$$\tau_0^2(\mathbf{x})|\nabla\tau_1(\mathbf{x})|^2 + 2\tau_0(\mathbf{x})\tau_1(\mathbf{x})\nabla\tau_0(\mathbf{x}) \cdot \nabla\tau_1(\mathbf{x}) + \tau_1^2(\mathbf{x})|\nabla\tau_0(\mathbf{x})|^2 = \frac{1}{v^2(\mathbf{x})}. \tag{23}$$

Once the gradient of the real part of the complex eikonal, $\nabla T(\mathbf{x})$, is available, we can use it as coefficients in the advection equation to compute the imaginary part of the complex eikonal. To treat the source singularity, we apply a multiplicative factorization to the imaginary part:

$$T^*(\mathbf{x}) = T(\mathbf{x})T_1^*(\mathbf{x}), \tag{24}$$

where T is the (just computed) real part of the complex eikonal capturing the source singularity, and the unknown perturbation factor T_1^* is computed by a finite-difference scheme. We remark in passing that, to capture the source singularity, we use T, which is solely related to the velocity, rather than Q, the reciprocal of which Q^{-1} may be zero near the source because the Q-based factorization may render T^* to be zero everywhere, which is ineffective. Following Qian et al. (2016), we also derive high-order factorization in Appendix A. Here, we use first-order factorization. Inserting equation 24 into equation 2, we obtain the factored advection equation:

$$T(\mathbf{x})\nabla T(\mathbf{x}) \cdot \nabla T_1^*(\mathbf{x}) + T_1^*(\mathbf{x})(\nabla T(\mathbf{x}))^2 = \frac{1}{v^2(\mathbf{x})Q(\mathbf{x})}. \tag{25}$$

Once the factorized Eulerian PDEs are derived, we can design finite-difference schemes to solve these equations.

Third-order LxF-WENO sweeping method

We will apply a third-order LxF-WENO sweeping method (Kao et al., 2004; Zhang et al., 2006; Qian et al., 2016) to solve the factored eikonal equation 23, in which high-order WENO approximations (Jiang and Peng, 2000; Qian et al., 2016) are essential for the success of the sweeping scheme. The third-order WENO scheme will yield real parts of the complex eikonal with high-order accuracy so that the numerical gradient $\nabla T(\mathbf{x})$ is also of high-order accuracy. Once the high-order accurate real part of the complex eikonal is obtained, we can use it as coefficients in the factored advection equation 25 so that a third-order LxF-WENO sweeping method can be applied to solve equation 25.

The LxF sweeping method (Kao et al., 2004; Zhang et al., 2006) offers a versatile and powerful approach for solving generic isotropic and anisotropic eikonal equations, such as quasi-P- and quasi-S-wave eikonal equations (Qian and Symes, 2001, 2002b). To simplify the presentation, we will only discuss 2D discretizations of equation 25, and similar strategies apply to the discretization of equation 23 (Qian et al., 2016). The extension to the 3D case is not difficult. To apply the LxF sweeping scheme to equation 25, we rewrite the equation into the following form:

$$H(x, z, T_1^*, p_{1x}^*, p_{1z}^*) = f, \tag{26}$$

where $p_{1x}^* = \partial T_1^*/\partial x$, $p_{1z}^* = \partial T_1^*/\partial z$, and the functions H and f are defined by, respectively,

$$H(x, z, T_1^*, p_{1x}^*, p_{1z}^*) = T(\mathbf{x})\nabla T(\mathbf{x}) \cdot \nabla T_1^*(\mathbf{x}) + T_1^*(\mathbf{x})(\nabla T(\mathbf{x}))^2, \tag{27}$$

$$f = \frac{1}{v^2(\mathbf{x})Q(\mathbf{x})}. \tag{28}$$

The third-order LxF-WENO sweeping method for T_1^* is defined by the following steps:

1) Initialization: The initialization is done by assigning values at a few grid points centered at the source point. In Appendix A, we provide a systematic high-order factorization for computing T_1^*. Here, we use the first-order factorization to assign these values. These values are fixed during iterations.

2) Iterations: Because T_1^* is computed by a third-order WENO scheme, we will use grid indexing (i.e., (i, j)) instead of spatial coordinates to demonstrate the iteration process. The LxF sweeping method computes T_1^* via Gauss-Seidel iteration with four alternating directions: (1) $i = 1:1:I$ and $j = 1:1:J$, (2) $i = 1:1:I$ and $j = J:-1:1$, (3) $i = I:-1:1$ and $j = 1:1:J$, and (4) $i = I:-1:1$ and $j = J:-1:1$, where i and j are the indices for the x- and z-coordinates, respectively, and I and J are the total number of grid points in the x- and z-directions, respectively.

At a grid point (i, j), the Lax-Friedrichs Hamiltonian (Osher and Shu, 1991; Kao et al., 2004) allows us to obtain a new value $T_1^{*\text{new}}$ from old values $T_1^{*\text{old}}$ in the following way:

$$\begin{aligned} T_1^{*\text{new}}(i,j) &= \left(\frac{1}{\frac{\alpha_x}{dx}+\frac{\alpha_z}{dz}}\right)\left(f(i,j) - H\left(i,j,T_1^{*\text{old}}(i,j), \frac{T_1^*(i+1,j)-T_1^*(i-1,j)}{2dx}, \frac{T_1^*(i,j+1)-T_1^*(i,j-1)}{2dz}\right)\right. \\ &\left. + \alpha_x\frac{T_1^*(i+1,j)+T_1^*(i-1,j)}{2dx} + \alpha_z\frac{T_1^*(i,j+1)+T_1^*(i,j-1)}{2dz}\right), \end{aligned} \tag{29}$$

where dx and dz are the grid sizes in the x- and z-directions, respectively, and α_x and α_z are the artificial viscosities in the x- and z-directions, respectively. Following Zhang et al. (2006), Qian et al. (2016), and Lu et al. (2016), we choose the following artificial viscosities:

$$\alpha_x = \max_{\Omega}\left(\left|\frac{\partial H}{\partial p_{1x}^*}\right| + \left|\frac{\partial H}{\partial T_1^*}\right|\right), \tag{30}$$

$$\alpha_z = \max_{\Omega}\left(\left|\frac{\partial H}{\partial p_{1z}^*}\right| + \left|\frac{\partial H}{\partial T_1^*}\right|\right), \tag{31}$$

where Ω is the entire computational domain. Following Zhang et al. (2006), we carry out the following replacement in equation 29 to introduce the third-order WENO approximation into the sweeping iteration:

$$T_1^*(i+1,j) = T_1^{*\text{old}}(i,j) + dx(p_{1x}^*(i,j))^+, \tag{32}$$

$$T_1^*(i-1,j) = T_1^{*\text{old}}(i,j) - dx(p_{1x}^*(i,j))^-, \tag{33}$$

$$T_1^*(i,j+1) = T_1^{*\text{old}}(i,j) + dz(p_{1z}^*(i,j))^+, \tag{34}$$

$$T_1^*(i,j-1) = T_1^{*\text{old}}(i,j) - dz(p_{1z}^*(i,j))^-, \tag{35}$$

where $(p_{1x}^*(i,j))^+$ and $(p_{1x}^*(i,j))^-$ are the third-order upwind WENO approximations of $p_{1x}^*(i,j)$ and $(p_{1z}^*(i,j))^+$ and $(p_{1z}^*(i,j))^-$ are the third-order upwind WENO approximations of $p_{1z}^*(i,j)$ (Jiang and Peng, 2000). The terms $(p_{1x}^*(i,j))^-$ and $(p_{1x}^*(i,j))^+$ are defined as follows:

$$(p_{1x}^*(i,j))^- = (1-\beta_-)\left(\frac{T_1^*(i+1,j)-T_1^*(i-1,j)}{2dx}\right) + \beta_-\left(\frac{3T_1^{*\text{old}}(i,j)-4T_1^*(i-1,j)+T_1^*(i-2,j)}{2dx}\right), \tag{36}$$

$$\beta_- = \frac{1}{1+2\gamma_-^2},$$
$$\gamma_- = \frac{\varepsilon + (T_1^{*\text{old}}(i,j) - 2T_1^*(i-1,j) + T_1^*(i-2,j))^2}{\varepsilon + (T_1^*(i+1,j) - 2T_1^{*\text{old}}(i,j) + T_1^*(i-1,j))^2}, \tag{37}$$

$$(p_{1x}^*(i,j))^+ = (1-\beta_+)\left(\frac{T_1^*(i+1,j)-T_1^*(i-1,j)}{2dx}\right) + \beta_+\left(\frac{-3T_1^{*\text{old}}(i,j)+4T_1^*(i+1,j)-T_1^*(i+2,j)}{2dx}\right), \tag{38}$$

$$\beta_+ = \frac{1}{1+2\gamma_+^2},$$
$$\gamma_+ = \frac{\varepsilon + (T_1^{*\text{old}}(i,j) - 2T_1^*(i+1,j) + T_1^*(i+2,j))^2}{\varepsilon + (T_1^*(i+1,j) - 2T_1^{*\text{old}}(i,j) + T_1^*(i-1,j))^2}; \tag{39}$$

similarly, we can define $(p_{1z}^*(i,j))^-$ and $(p_{1z}^*(i,j))^+$.

3) **Convergence:** If the following condition is satisfied,

$$|T_1^{*\text{new}}(i,j) - T_1^{*\text{old}}(i,j)| \le \delta, \tag{40}$$

the iteration converges and we terminate the iteration, where δ is a predefined threshold value.

Once T_1^* is computed, the imaginary part is available from equation 24. Compared with a first-order scheme, a high-order scheme can yield the corresponding numerical derivatives with high-order accuracy in the Eulerian PDEs. Therefore, to achieve a certain specified accuracy, a high-order scheme only needs to use a much coarser mesh than a first-order scheme does (Qian and Symes, 2002a; Luo et al., 2014); because the number of grid points is greatly reduced, the computational cost can be reduced (Qian and Symes, 2002a; Luo et al., 2014). This consideration justifies our choice of using a high-order WENO scheme here.

NUMERICAL EXPERIMENTS

Eulerian examples for viscoacoustic ray tracing

We apply our proposed algorithm to four cases of the viscoacoustic attenuating model, in which the model is prescribed by a real-valued acoustic velocity and a real-valued quality factor.

For the first case, we choose a velocity v with a constant vertical gradient. The velocity model is specified by $v = 2000.0 + 0.5z$ (m/s). The Q model is homogeneous with $Q = 50$. Because Červený (2001) provides an analytic solution of the eikonal equation 1 for this constant-gradient velocity model, we may use this solution to validate our algorithm for the eikonal equation. Moreover, because the Q model is homogeneous, the exact solution of the advection equation 2 can be obtained by dividing the exact traveltime by the Q value according to equations 5 and 6. The model dimension is 5 km in depth and 5 km laterally. One advantage of high-order WENO approximations is their high accuracy, which allows us to solve the eikonal and advection equations using large grid sizes. Therefore, we use a grid size of 50 m in the x- and z-directions. The total number of grids is 101×101. We place a source at $x = 2500$ m and $z = 0$ m. Figure 1a and 1b shows the computed real and imaginary parts of the complex eikonal for the first attenuating model, respectively. To validate their accuracies, we compare numerical solutions with the corresponding analytic solutions, as shown in Figure 1c and 1d. The errors in the computed real part are of a magnitude of 10^{-6}, which is much smaller than a time sampling interval, such as 1 ms in a typical seismic record. The errors in the imaginary part of the complex eikonal are of a magnitude of 10^{-7}, which is also quite accurate. This shows that the proposed method yields highly accurate complex eikonals under the weakly attenuating approximation for this case.

In the second case, the velocity model as shown in Figure 2a is extracted from the BP tilted transversely isotropic velocity model. We further construct a Q model according to the extracted velocity model: we fill the zone of low velocity in the shallow region with low Q values to simulate the gas cloud, and we set the Q value in other places to be 10,000 (as shown in Figure 2b). Note that in displaying Figure 2b, we clip the maximum Q value to 100. The model dimension is 8 km in depth and 10 km laterally. The grid size is 50 m in the x- and z-directions. The total number of grid points is 201×161. The source is located at $x = 5000$ m and $z = 0$ m. The proposed method is used to compute the real and imaginary parts of the complex eikonal, as shown in Figure 3. The imaginary part of the eikonal in Figure 3b shows that only raypaths passing through the gas cloud suffer from dispersion and absorption, where the maximum value of the imaginary part is approximately 5 ms. This demonstrates the strong seismic attenuation below the gas cloud. Because in this inhomogeneous attenuating model we do not have an analytic solution to validate the result, we use the wavefield snapshot obtained by a finite-difference wavefield extrapolator to validate the real part of the complex eikonal. The wavefield snapshot is obtained on a grid with a mesh size of 10 m in the

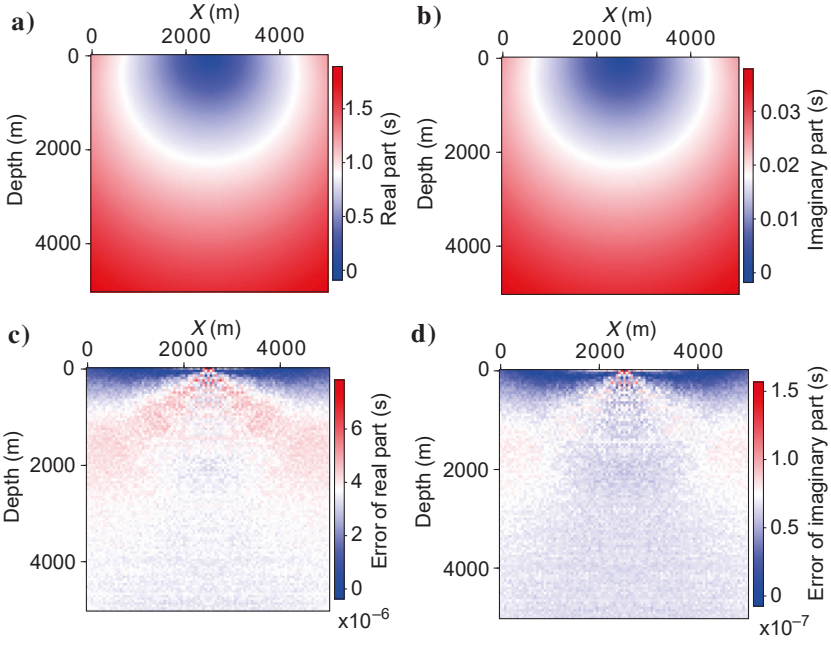

Figure 1. The real and imaginary parts of the complex-valued eikonal for the constant-gradient velocity model. (a) The real part and (c) its difference with the analytic solution. (b) The imaginary part and (d) its difference with the analytic solution under the weakly attenuating approximation.

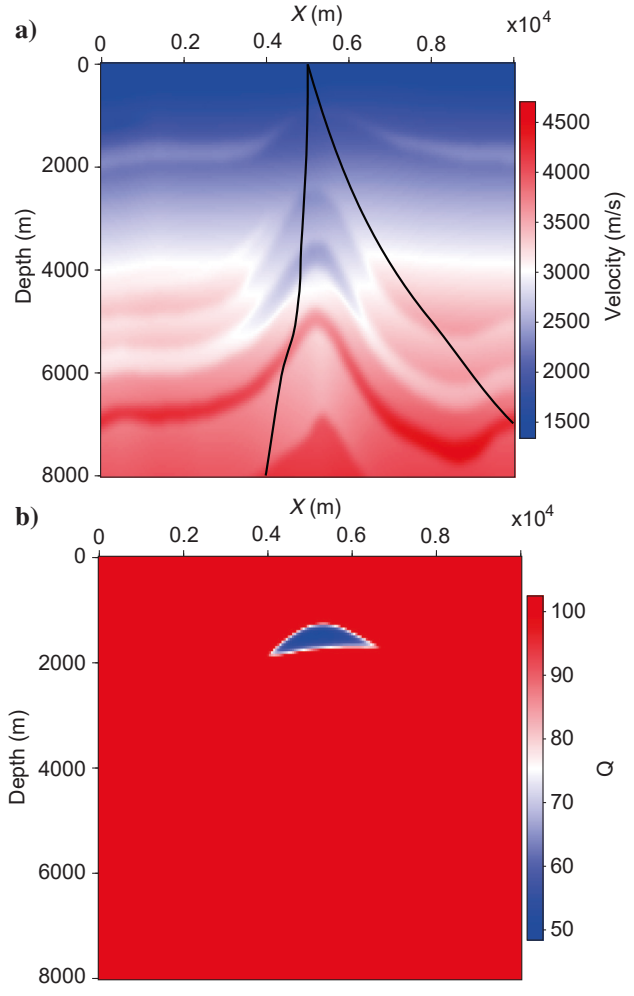

Figure 2. An attenuation model with a gas cloud. (a) The acoustic velocity and (b) Q. The two black curves in (a) are two raypaths with the takeoff angles being 0° and 20°.

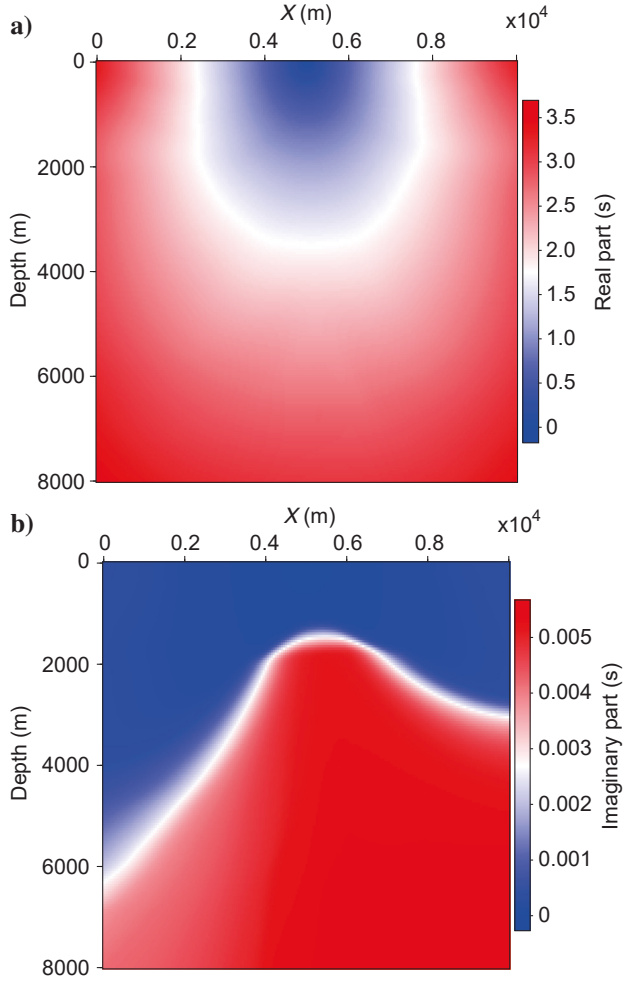

Figure 3. The real and imaginary parts of the complex-valued eikonal for the gas clouded attenuating model. (a) The real part and (b) the imaginary part.

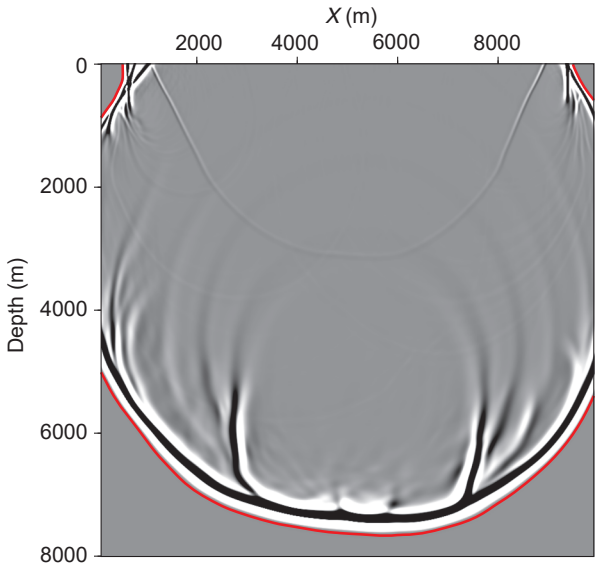

Figure 4. Wavefield snapshot overlaid by the contour of the real part at 3 s. The red curve is the contour of the real part.

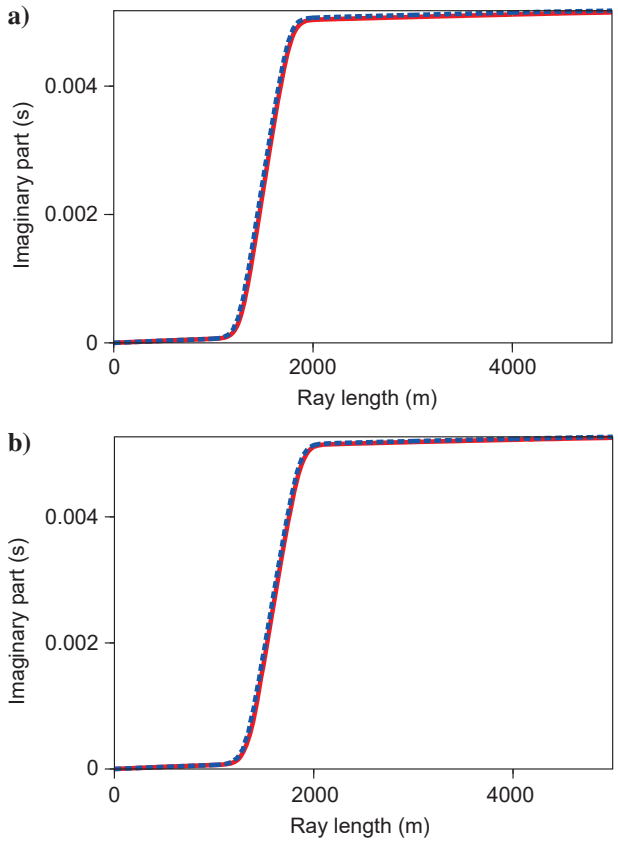

Figure 5. Comparison between the imaginary parts obtained by the Eulerian PDE method and the ray-tracing method for the gas clouded attenuating model. The imaginary part for rays with (a) 0° and (b) 20° takeoff angle. The red curve and blue dotted curve are the imaginary parts obtained by the ray-tracing method and the Eulerian PDE method, respectively.

x- and z-directions. Figure 4 shows the wavefield snapshot overlaid by the contour of the computed real part of the eikonal at 3 s, where the red curve is the contour of the real part. Because the contour of the real part matches well with the first-arrival wavefront in the wavefield snapshot, this demonstrates that the real part of the eikonal is highly accurate, even though it is computed on a grid of relatively large mesh size. To validate the computed imaginary part, we carry out ray tracings with a fourth-order Runge-Kutta ODE integrator to obtain imaginary parts along two raypaths, where the two black curves shown in Figure 2a pass through the gas cloud. Here, the ray tracing is performed on a fine grid with a mesh size of 10 m. We use a nonlinear interpolation method to obtain the imaginary parts along these two raypaths from the result shown in Figure 3b. The comparison between the imaginary parts obtained by the proposed method and the ray-tracing method is shown in Figure 5, and the two results match well. This shows that the imaginary part obtained by the proposed method is highly accurate under the weakly attenuating approximation. In addition, Figure 5 also shows that the attenuation increases rapidly as seismic rays pass through the gas cloud.

In the third case, we build an attenuating model based on a land scenario, in which the velocity and Q models are shown in Figure 6.

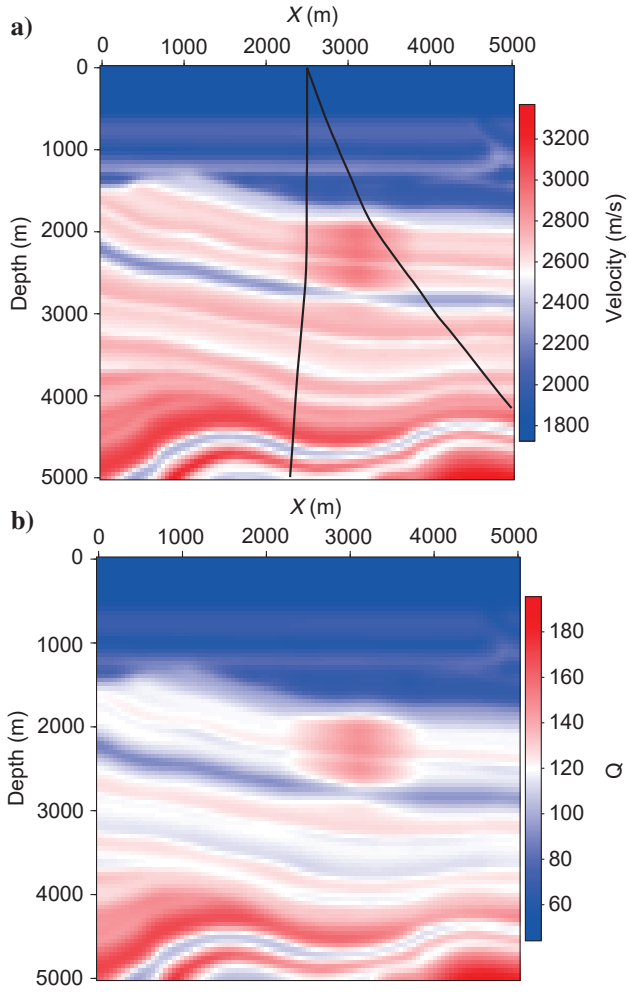

Figure 6. The attenuation model for a land scenario. (a) Acoustic velocity and (b) Q. Two black curves in (a) are two raypaths with the takeoff angles being 0° and 20°.

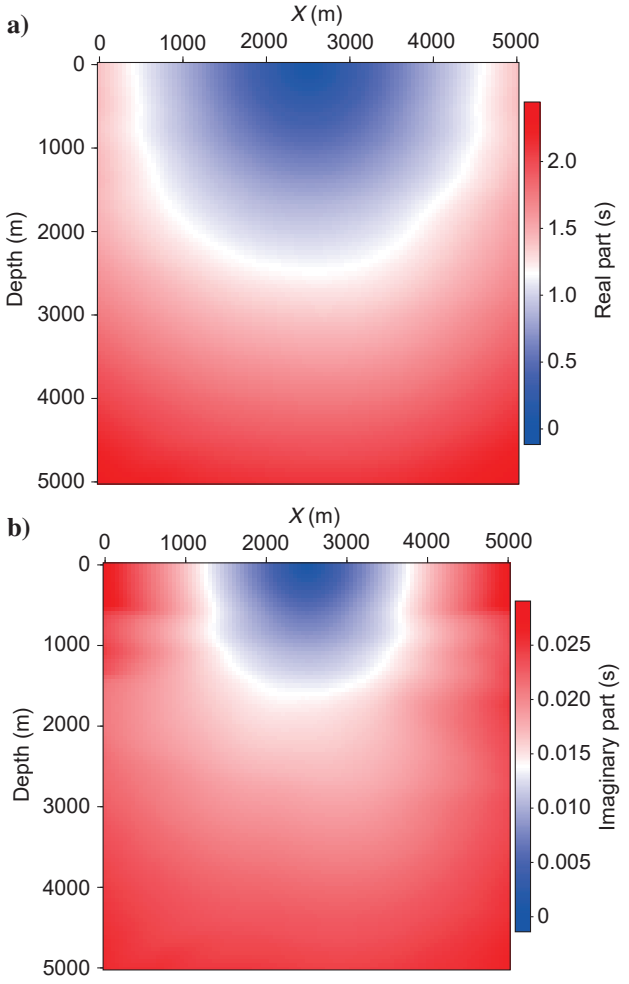

Figure 7. The real and imaginary parts of the complex-valued eikonal for the land attenuating model. (a) The real part and (b) the imaginary part.

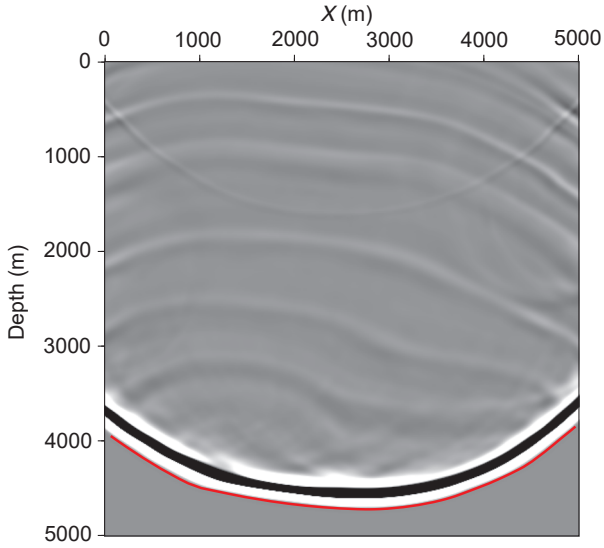

Figure 8. Wavefield snapshot overlaid by the contour of the real part at 2 s. The red curve is the contour of the real part.

In the Q model, the Q value is very low in the shallow area to simulate the strong attenuation caused by the near-surface region. The model dimensions are 5 km in depth and 5 km laterally. The grid size is 50 m in the x- and z-directions. The total number of mesh points is 101×101. The source is located at $x = 2500$ m and $z = 0$ m. Figure 7 shows the computed real and imaginary parts of the complex eikonal by the proposed method. The maximum value of the imaginary part in Figure 7b is approximately 30 ms, which shows a very strong attenuation due to the low Q zone in the near-surface region. To validate the result, we also use a wavefield snapshot and a ray-tracing result on a fine grid with mesh size of 10 m. Figure 8 shows the wavefield snapshot overlaid by the contour of the real part at 2 s, where the contour matches well with the first-arrival wavefront in the wavefield snapshot. Figure 9 shows a comparison between the imaginary parts obtained by the proposed method and the ray-tracing method along two raypaths as shown in Figure 6a, and these two results match well. This demonstrates that the proposed method produces highly accurate complex eikonals under the weakly attenuating approximation.

In the fourth case, we show a 3D example. We build a 3D inhomogeneous attenuating model with the velocity and Q varying vertically. The velocity and Q models are specified by $v = 1500.0 + 0.5z$ (m/s) and $Q = 50 + 0.016z$, respectively. The model dimension is 5 km in the x-, y-, and z-directions. The grid size is

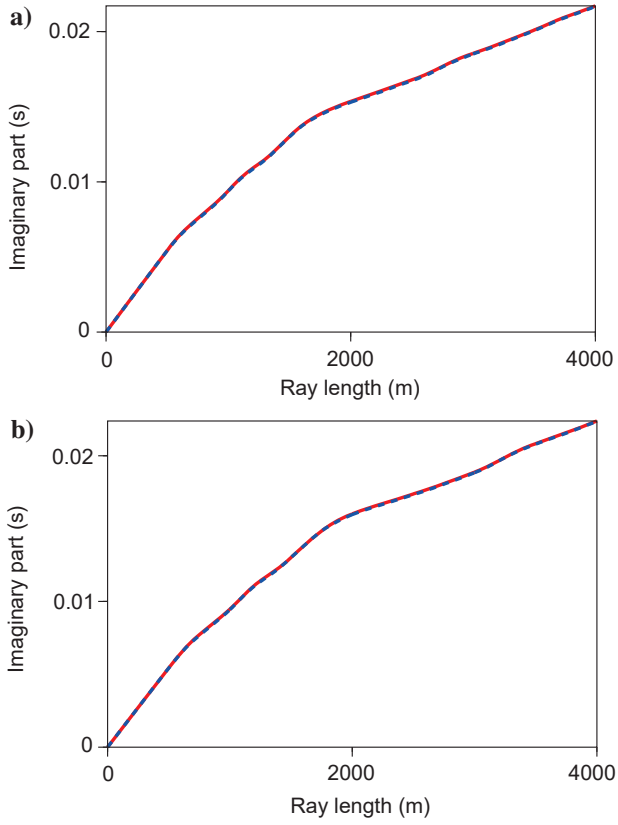

Figure 9. Comparison between the imaginary parts obtained by the Eulerian PDE method and the ray-tracing method for the land attenuating model. The imaginary parts for rays with (a) 0° and (b) 20° takeoff angle. The red curve and the blue dotted curve are the imaginary parts obtained by the ray-tracing method and the Eulerian PDE method, respectively.

50 m in the x-, y-, and z-directions. The total number of mesh points is $101 \times 101 \times 101$. The source is located at $x = 2500$ m, $y = 2500$ m, and $z = 0$ m. Figure 10 shows the computed real and imaginary parts of the complex eikonal by the proposed method. This demonstrates that the proposed method performs well in 3D applications.

Eulerian examples for real-elastic and real-viscoelastic ray tracing

We now apply our proposed real-elastic and viscoelastic Eulerian PDE methods to a particular velocity-attenuation model in Vavryčuk (2012), which is smoothly inhomogeneous with a constant gradient of the square of the complex slowness. The model is specified by

$$c^{-2}(\mathbf{x}) = v_0^{-2} + A_x x + A_z z, \tag{41}$$

where v_0 is the background velocity and A_x and A_z are the gradients in the x- and z-directions, respectively. This complex velocity can also be converted into v and Q in equations 1 and 2 accordingly. Vavryčuk (2012) also proposes an analytic solution of the complex eikonal to this model by using complex ray tracing.

In our computation, we set the model dimension to be 4 km in depth and 10 km laterally. We choose the grid size to be 50 m in the x- and z-directions, so that the total number of mesh points is 81×201. The source is located at $x = 0$ m and $z = 0$ m. We consider two cases, case A and case B.

In case A, $v_0 = 1$ km/s, $A_x = 0.1i$, $A_z = 0.0$, and the complex velocity is shown in Figure 11. This model is relatively simple with only a lateral gradient along the x-direction, but its quality factor can take a value as low as one, which represents strong attenuation.

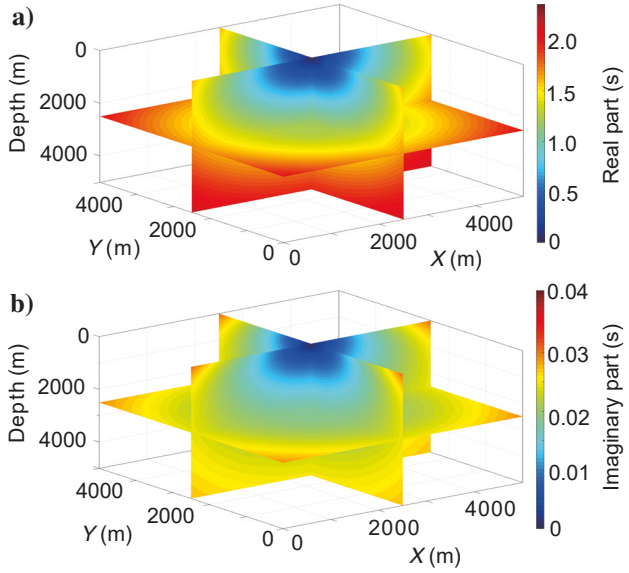

Figure 10. The real and imaginary parts of the complex-valued eikonal for the 3D model. (a) The real part and (b) the imaginary part.

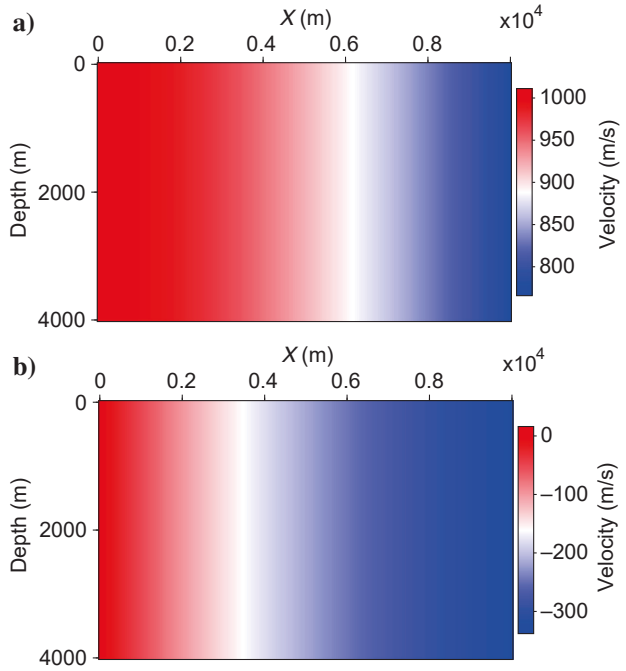

Figure 11. (a) The real and (b) imaginary parts of the complex velocity in case A.

Figure 12. The complex-valued eikonal for the real-elastic Eulerian PDE method in case A. (a) The real part and (c) its difference with the analytic solution. (b) The imaginary part and (d) its difference with the analytic solution.

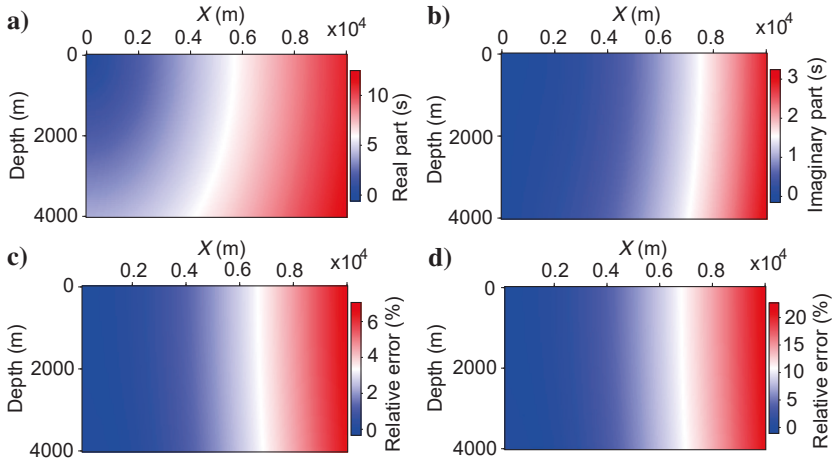

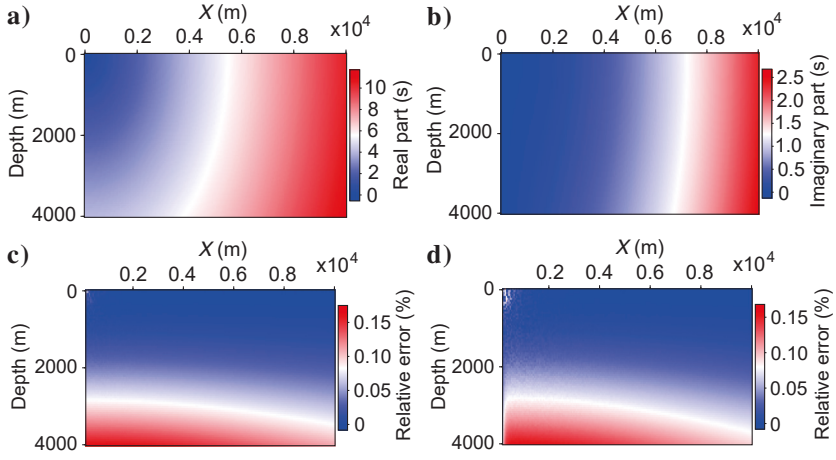

Figure 13. The complex-valued eikonal for the real-viscoelastic Eulerian PDE method in case A. (a) The real part and (c) its difference with the analytic solution. (b) The imaginary part and (d) its difference with the analytic solution.

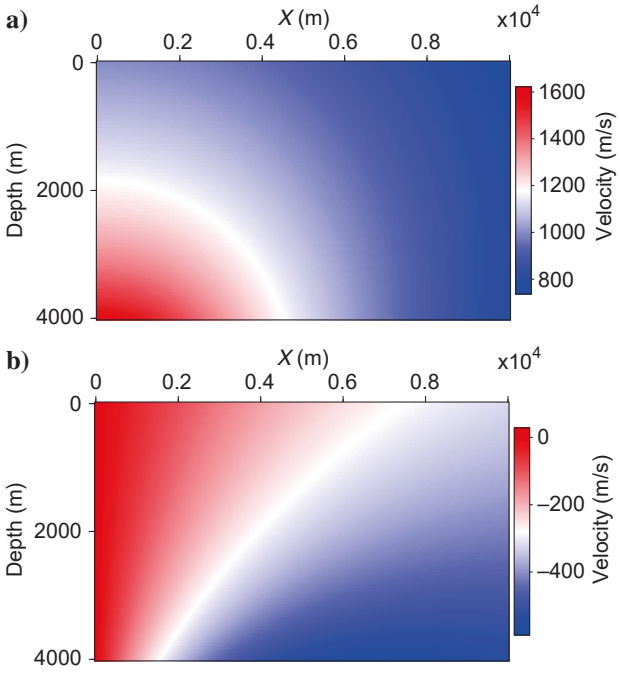

Figure 14. (a) Real and (b) imaginary parts of the complex velocity in case B.

Figures 12 and 13 are the real and imaginary parts of the complex eikonal computed by our real-elastic and real-viscoelastic Eulerian methods, respectively. To validate these computed results, we also compute their differences with the corresponding analytic solution. Note that we denote these differences according to the relative errors to make them comparable with those in Vavryčuk (2012). The differences in Figures 12 and 13 show that the errors from the real-viscoelastic Eulerian method are less than 0.2%, and the real-viscoelastic Eulerian method yields higher accuracy than the real-elastic Eulerian method in this strongly attenuating model. The differences in Figures 12 and 13 are also comparable with those in Vavryčuk (2012), which shows that the proposed methods can produce results comparable with those from the corresponding ray-tracing methods.

In case B, $v_0 = 1$ km/s, $A_x = 0.1i$, $A_z = -0.15$, and the complex velocity is shown in Figure 14. This model becomes more complicated due to the nonzero gradients in the x- and z-directions, and it also represents strong attenuation. Figures 15 and 16 show the real and imaginary parts of the complex-valued eikonal computed by the real-elastic and real-viscoelastic Eulerian methods, respectively. We also compute their differences with the corresponding analytic solutions. Similarly, in comparison with the solution provided by the exact complex ray tracing, the real-viscoelastic Eulerian method yields higher accuracy than the real-elastic Eulerian method. Comparing the errors in case B with those in case

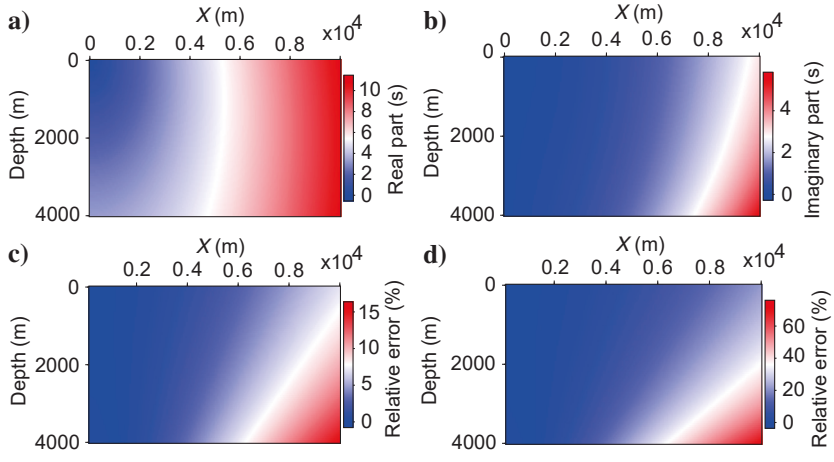

Figure 15. The complex-valued eikonal for the real-elastic Eulerian PDE method in case B. (a) The real part and (c) its difference with the analytic solution. (b) The imaginary part and (d) its difference with the analytic solution.

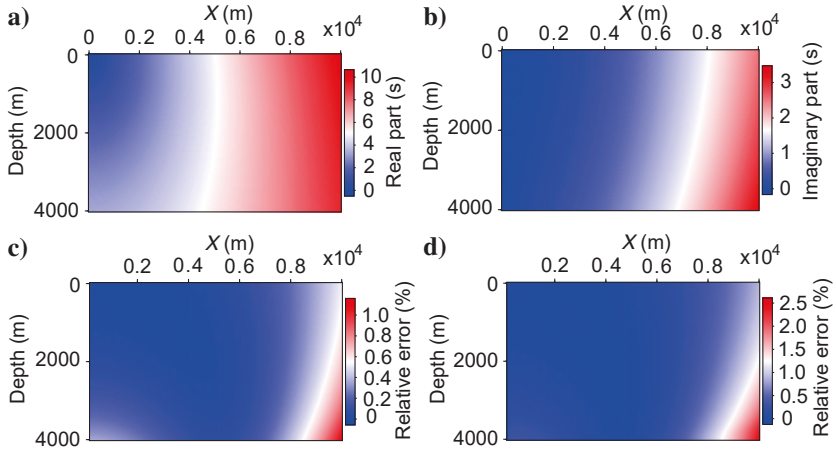

Figure 16. The complex-valued eikonal for the real-viscoelastic Eulerian PDE method in case B. (a) The real part and (c) its difference with the analytic solution. (b) The imaginary part and (d) its difference with the analytic solution.

A, we can conclude that the approximation error due to the real-space modeling increases as the model complexity in attenuation increases. The differences in Figures 15 and 16 are also comparable with those in Vavryčuk (2012), which shows that the proposed methods can produce results comparable with those from the corresponding ray-tracing methods.

CONCLUSION

Computing complex-valued eikonals efficiently in attenuating media is essential for seismic imaging and tomography. We propose a Eulerian PDE method to compute complex-valued eikonals in attenuating media as an alternative solution to the ray-tracing method. One major advantage of the proposed Eulerian method is that it computes complex-valued eikonals on regular grids, which can be directly used by imaging and tomography methods. Our proposed method uses two Eulerian PDEs to govern the evolution of the real and imaginary parts of complex-valued eikonals. The real-space eikonal equation governs the evolution of the real part of the complex-valued eikonal, and a novel real-space advection equation governs the evolution of the imaginary part of the complex-valued eikonal. The factorization strategy is further applied to obtain factorized Eulerian PDEs to treat source singularities. Furthermore, a third-order LxF WENO sweeping method is proposed to solve these Eulerian PDEs. We applied the proposed Eulerian method to several attenuation models and have obtained satisfying results.

ACKNOWLEDGMENTS

Hu and Cao appreciate the financial support from the National Natural Science Foundation of China (grant nos. 42074166, 42030812, and 41974160). Qian is partially supported by the National Science Foundation (grant nos. 1614566 and 2012046). Leung is partially supported by the Hong Kong RGC (grant no. 16302819). The authors thank BP plc for the benchmark synthetic model. We thank J. Shragge, C. Torres-Verdin, Y. Liu, X. Huang, A. Stovas, and the three anonymous reviewers for their helpful comments and suggestions.

DATA AND MATERIALS AVAILABILITY

Data associated with this research are available and can be obtained by contacting the corresponding author.

APPENDIX A

HIGH-ORDER FACTORIZATION FOR COMPUTING T^*

According to ray theory, we have the following relation from the eikonal equation 1 and the advection equation 2:

$$\frac{dT}{ds} = \frac{1}{v}, \quad \frac{dT^*}{ds} = \frac{1}{vQ}, \tag{A-1}$$

where d/ds corresponds to the tangential derivative along a raypath and s is the arc length.

When v and Q are constants, we can obtain the relation between T and T^*: $T^* = (1/Q)T$. Therefore, to compute high-order approximations to T^* near the source (here set at the origin), we factorize T^* as

$$T^* = TT_1^*, \tag{A-2}$$

where the singularity of T^* at the source is captured by T, and so the underlying factor T_1^* is smooth in the neighborhood of the source.

Inserting the above factorization into equation 2 and multiplying both sides by two, we can obtain the corresponding equation for T_1^*:

$$\nabla T^2 \cdot \nabla T_1^* + \frac{2}{v^2} T_1^* = \frac{2}{v^2 Q}. \tag{A-3}$$

Assuming that $1/v^2$ and $1/Q$ are smooth, we can expand T^2, T_1^*, $1/v^2$, and $1/Q$ into a power series near the source as illustrated in Qian et al. (2016):

$$T^2 = \sum_{\nu=0}^{\infty} T_k; \quad T_1^* = \sum_{\nu=0}^{\infty} U_k; \quad \frac{1}{v^2} = \sum_{\nu=0}^{\infty} S_k; \quad \frac{1}{Q} = \sum_{\nu=0}^{\infty} Q_k. \tag{A-4}$$

DOI:10.1190/geo2020-0659.1

The term T_k is given in Qian et al. (2016), and we know that $T_0 = 0$, $T_1 = 0$, and $T_2 = S_0|\mathbf{x}|^2$. Inserting the above expansions into equation A-3, we can get

$$\left(\sum_{\nu=2}^{\infty}\nabla T_k\right)\cdot\left(\sum_{\nu=0}^{\infty}\nabla U_k\right)+2\left(\sum_{\nu=0}^{\infty}S_k\right)\left(\sum_{\nu=0}^{\infty}U_k\right)=2\left(\sum_{\nu=0}^{\infty}S_k\right)\left(\sum_{\nu=0}^{\infty}Q_k\right). \tag{A-5}$$

We can now equate the pth degree terms to get the following recursive equation:

$$\sum_{\nu=0}^{p}\nabla T_{p-v+2}\cdot\nabla U_\nu+2\sum_{\nu=0}^{p}S_{p-\nu}U_\nu=2\sum_{\nu=0}^{p}S_vQ_{p-\nu}. \tag{A-6}$$

Using the relation $T_2 = S_0|\mathbf{x}|^2$ and $\nabla T_2\cdot\nabla U_p = 2pS_0U_p$, we can obtain the following recursive formulas for $\{U_p\}$ for $p \geq 0$:

$$2(p+1)S_0U_p=2\sum_{\nu=0}^{p}S_vQ_{p-\nu}-\sum_{\nu=0}^{p-1}\nabla T_{p-v+2}\cdot\nabla U_\nu-2\sum_{\nu=0}^{p-1}S_{p-\nu}U_\nu. \tag{A-7}$$

We list some special cases for $p = 0, 1, 2, 3, 4$, respectively:

$$p=0{:}\,2S_0U_0=2S_0Q_0\Rightarrow U_0=Q_0, \tag{A-8}$$

$$p=1{:}\,4S_0U_1=2S_0Q_1+2S_1Q_0-2S_1U_0\Rightarrow U_1=\frac{1}{2}Q_1, \tag{A-9}$$

$$p=2{:}\,6S_0U_2=2(S_0Q_2+S_1Q_1+S_2Q_0)-\nabla T_3\cdot\nabla U_1-2(S_2U_0+S_1U_1)\Rightarrow U_2=\frac{Q_2}{3}+\frac{S_1Q_1}{6S_0}-\frac{\nabla T_3\cdot\nabla Q_1}{12S_0}, \tag{A-10}$$

$$p=3{:}\,8S_0U_3=2(S_0Q_3+S_1Q_2+S_2Q_1+S_3Q_0)-\nabla T_4\cdot\nabla U_1-\nabla T_3\cdot\nabla U_2-2(S_3U_0+S_2U_1+S_1U_2)\Rightarrow U_3=\frac{Q_3}{4}+\frac{S_1Q_2}{4S_0}+\frac{S_2Q_1}{8S_0}-\frac{S_1U_2}{4S_0}-\frac{\nabla T_4\cdot\nabla Q_1}{16S_0}-\frac{\nabla T_3\cdot\nabla U_2}{8S_0}, \tag{A-11}$$

$$p=4{:}\,10S_0U_4=2(S_0Q_4+S_1Q_3+S_2Q_2+S_3Q_1+S_4Q_0)-\nabla T_5\cdot\nabla U_1-\nabla T_4\cdot\nabla U_2-\nabla T_3\cdot\nabla U_3-2(S_4U_0+S_3U_1+S_2U_2+S_1U_3)\Rightarrow U_4=\frac{Q_4}{5}+\frac{S_1Q_3}{5S_0}+\frac{S_2Q_2}{5S_0}+\frac{S_3Q_1}{10S_0}-\frac{S_2U_2}{5S_0}-\frac{S_1U_3}{5S_0}-\frac{\nabla T_5\cdot\nabla Q_1}{20S_0}-\frac{\nabla T_4\cdot\nabla U_2}{10S_0}-\frac{\nabla T_3\cdot\nabla U_3}{10S_0}. \tag{A-12}$$

REFERENCES

Aki, K., and P. Richards, 1980, Quantitative seismology: Freeman and Co.

Blanch, J. O., and J. O. A. Robertsson, 1997, A modified Lax-Wendroff correction for wave propagation in media described by Zener elements: Geophysical Journal International, **131**, 381–386, doi: 10.1111/j.1365-246X.1997.tb01229.x.

Blanch, J. O., J. O. A. Robertsson, and W. W. Symes, 1995, Modeling of a constant Q: Methodology and algorithm for an efficient and optimally inexpensive viscoelastic technique: Geophysics, **60**, 176–184, doi: 10.1190/1.1443744.

Carcione, J. M., 1999, Staggered mesh for the anisotropic and viscoelastic wave equation: Geophysics, **64**, 1863–1866, doi: 10.1190/1.1444692.

Carcione, J. M., 2009, Theory and modeling of constant-Q P- and S-waves using fractional time derivatives: Geophysics, **74**, no. 1, T1–T11, doi: 10.1190/1.3008548.

Carcione, J. M., 2015, Wave fields in real media: Theory and numerical simulation of wave propagation in anisotropic, anelastic, porous and electromagnetic media: Handbook of geophysical exploration, 3rd ed.: Elsevier.

Carcione, J. M., F. Cavallini, F. Mainardi, and A. Hanyga, 2002, Time domain seismic modeling of constant-Q wave propagation using fractional derivatives: Pure and Applied Geophysics, **159**, 1719–1736, doi: 10.1007/s00024-002-8705-z.

Červený, V., 2001, Seismic ray theory: Cambridge University Press.

Fomel, S., S. Luo, and H. K. Zhao, 2009, Fast sweeping method for the factored eikonal equation: Journal of Computational Physics, **228**, 6440–6455, doi: 10.1016/j.jcp.2009.05.029.

Futterman, W., 1962, Dispersive body waves: Journal of Geophysical Research, **67**, 5279–5291, doi: 10.1029/JZ067i013p05279.

Gajewski, D., and I. Pšenčik, 1992, Vector wavefields for weakly attenuating anisotropic media by the ray method: Geophysics, **57**, 27–38, doi: 10.1190/1.1443186.

Hao, Q., and T. Alkhalifah, 2017, An acoustic eikonal equation for attenuating transversely isotropic media with a vertical symmetry axis: Geophysics, **82**, no. 1, C9–C20, doi: 10.1190/geo2016-0160.1.

Hu, J. T., P. Wang, J. X. Cao, H. Z. Wang, and X. J. Wang, 2018, Frequency dependent complex traveltime computation in TI media with weak attenuation using Fermat's principle based fast marching: 88th Annual International Meeting, SEG, Expanded Abstracts, 4040–4044, doi: 10.1190/segam2018-2998299.1.

Huang, X., and S. Greenhalgh, 2018, Linearized formulations and approximate solutions for the complex eikonal equation in orthorhombic media and applications of complex seismic traveltime: Geophysics, **83**, no. 3, C115–C136, doi: 10.1190/geo2017-0620.1.

Huang, X., J. Sun, and S. Greenhalgh, 2018, On the solution of the complex eikonal equation in acoustic VTI media: A perturbation plus optimization scheme: Geophysical Journal International, **214**, 907–932, doi: 10.1093/gji/ggy159.

Jiang, G. S., and D. Peng, 2000, Weighted ENO schemes for Hamilton-Jacobi equations: SIAM Journal on Scientific Computing, **21**, 2126–2143, doi: 10.1137/S106482759732455X.

Kao, C. Y., S. J. Osher, and J. Qian, 2004, Lax-Friedrichs sweeping schemes for static Hamilton-Jacobi equations: Journal of Computational Physics, **196**, 367–391, doi: 10.1016/j.jcp.2003.11.007.

Kao, C. Y., S. J. Osher, and J. Qian, 2008, Legendre transform based fast sweeping methods for static Hamilton-Jacobi equations on triangulated meshes: Journal of Computational Physics, **227**, 10209–10225, doi: 10.1016/j.jcp.2008.08.016.

Keers, H., D. W. Vasco, and L. R. Johnson, 2001, Viscoacoustic crosswell imaging using asymptotic waveforms: Geophysics, **66**, 861–870, doi: 10.1190/1.1444975.

Kim, S., and R. Cook, 1999, 3-D traveltime computation using second-order ENO scheme: Geophysics, **64**, 1867–1876, doi: 10.1190/1.1444693.
Klimeš, M., and L. Klimeš, 2011, Perturbation expansions of complex-valued traveltime along real-valued reference rays: Geophysical Journal International, **186**, 751–759, doi: 10.1111/j.1365-246X.2011.05054.x.
Lions, P. L., 1982, Generalized solutions of Hamilton-Jacobi equations: Pitman Advanced Publishing Program.
Lu, W., J. Qian, and R. Burridge, 2016, Babich's expansion and the fast Huygens sweeping method for the Helmholtz wave equation at high frequencies: Journal of Computational Physics, **313**, 478–510, doi: 10.1016/j.jcp.2016.02.048.
Luo, S., and J. Qian, 2012, Fast sweeping methods for factored anisotropic eikonal equations: Multiplicative and additive factors: Journal of Scientific Computing, **52**, 360–382, doi: 10.1007/s10915-011-9550-y.
Luo, S., J. Qian, and R. Burridge, 2014, High-order factorization based high-order hybrid fast sweeping methods for point-source eikonal equations: SIAM Journal on Numerical Analysis, **52**, 23–44, doi: 10.1137/120901696.
Osher, S. J., and C. W. Shu, 1991, High-order essentially nonoscillatory schemes for Hamilton-Jacobi equations: SIAM Journal on Numerical Analysis, **28**, 907–922, doi: 10.1137/0728049.
Pica, A., 1997, Fast and accurate finite-difference solutions of the 3-D eikonal equation parameterized in celerity: 67th Annual International Meeting, SEG, Expanded Abstracts, 1774–1777, doi: 10.1190/1.1885777.
Podvin, P., and I. Lecomte, 1991, Finite difference computation of traveltimes in very contrasted velocity models: A massively parallel approach and its associated tools: Geophysical Journal International, **105**, 271–284, doi: 10.1111/j.1365-246X.1991.tb03461.x.
Qian, J., and W. W. Symes, 2001, Paraxial eikonal solvers for anisotropic quasi-P traveltimes: Journal of Computational Physics, **173**, 256–278, doi: 10.1006/jcph.2001.6875.
Qian, J., and W. W. Symes, 2002a, An adaptive finite difference method for traveltime and amplitude: Geophysics, **67**, 167–176, doi: 10.1190/1.1451472.
Qian, J., and W. W. Symes, 2002b, Finite-difference quasi-P traveltimes for anisotropic media: Geophysics, **67**, 147–155, doi: 10.1190/1.1451438.
Qian, J., L. Yuan, Y. Liu, S. Luo, and R. Burridge, 2016, Babich's expansion and high-order Eulerian asymptotics for point-source Helmholtz equations: Journal of Scientific Computing, **67**, 883–908, doi: 10.1007/s10915-015-0111-7.
Qian, J., Y. T. Zhang, and H. K. Zhao, 2007a, Fast sweeping methods for eikonal equations on triangulated meshes: SIAM Journal on Numerical Analysis, **45**, 83–107, doi: 10.1137/050627083.
Qian, J., Y. T. Zhang, and H. K. Zhao, 2007b, Fast sweeping methods for static convex Hamilton-Jacobi equations: Journal of Scientific Computing, **31**, 237–271, doi: 10.1007/s10915-006-9124-6.
Qin, F., Y. Luo, K. B. Olsen, W. Cai, and G. T. Schuster, 1992, Finite difference solution of the eikonal equation along expanding wavefronts: Geophysics, **57**, 478–487, doi: 10.1190/1.1443263.
Robertsson, J. O. A., J. O. Blanch, and W. W. Symes, 1994, Viscoelastic finite-difference modeling: Geophysics, **59**, 1444–1456, doi: 10.1190/1.1443701.
Serna, S., and J. Qian, 2010, A stopping criterion for higher-order sweeping schemes for static Hamilton-Jacobi equations: Journal of Computational Mathematics, **28**, 552–568, doi: 10.4208/jcm.1003-m0016.
Sethian, J. A., and A. M. Popovici, 1999, 3-D traveltime computation using the fast marching method: Geophysics, **64**, 516–523, doi: 10.1190/1.1444558.
van Trier, J., and W. W. Symes, 1991, Upwind finite-difference calculation of traveltimes: Geophysics, **56**, 812–821, doi: 10.1190/1.1443099.
Vavryčuk, V., 2008a, Real ray tracings in anisotropic viscoelastic media: Geophysical Journal International, **175**, 617–626, doi: 10.1111/j.1365-246X.2008.03898.x.
Vavryčuk, V., 2008b, Velocity, attenuation and quality factor in anisotropic viscoelastic media: A perturbation approach: Geophysics, **73**, no. 5, D63–D73, doi: 10.1190/1.2921778.
Vavryčuk, V., 2012, On numerically solving the complex eikonal equation using real ray-tracing methods: A comparison with the exact analytical solution: Geophysics, **77**, no. 4, T109–T116, doi: 10.1190/geo2011-0431.1.
Vidale, J., 1988, Finite-difference calculation of travel times: Bulletin of the Seismological Society of America, **78**, 2062–2076.
Waheed, U., C. E. Yarman, and G. Flagg, 2015, An iterative, fast-sweeping-based eikonal solver for 3D tilted anisotropic media: Geophysics, **80**, no. 3, C49–C58, doi: 10.1190/geo2014-0375.1.
Xie, Y., J. Sun, Y. Zhang, and J. Zhou, 2015, Compensating for visco-acoustic effects in TTI reverse time migration: 85th Annual International Meeting, SEG, Expanded Abstracts, 3996–4001, doi: 10.1190/segam2015-5855445.1.
Xie, Y., K. Xin, J. Sun, and C. Notfors, 2009, 3D prestack depth migration with compensation for frequency dependent absorption and dispersion: 79th Annual International Meeting, SEG, Expanded Abstracts, 2919–2913, doi: 10.3997/2214-4609-pdb.255.52.
Xin, K. F., Y. He, Y. Xie, W. Q. Xu, and M. Wang, 2014, Robust Q tomographic inversion through adaptive extraction of spectral features: 84th Annual International Meeting, SEG, Expanded Abstracts, 3726–3730, doi: 10.1190/segam2014-0421.1.
Zhang, L., J. W. Rector, and G. M. Hoversten, 2005, Eikonal solver in the celerity domain: Geophysical Journal International, **162**, 1–8, doi: 10.1111/j.1365-246X.2005.02626.x.
Zhang, Y., P. Zhang, and H. Zhang, 2010, Compensating for visco-acoustic effects in reverse time migration: 80th Annual International Meeting, SEG, Expanded Abstracts, 3160–3164, doi: 10.1190/1.3513503.
Zhang, Y. T., H. K. Zhao, and J. Qian, 2006, High order fast sweeping methods for static Hamilton-Jacobi equations: Journal of Scientific Computing, **29**, 25–56, doi: 10.1007/s10915-005-9014-3.
Zhao, H. K., 2005, Fast sweeping method for eikonal equations: Mathematics of Computation, **74**, 603–628, doi: 10.1090/S0025-5718-04-01678-3.

Biographies and photographs of the authors are not available.